

**Coupling Effects Between Metal-organic Framework Derivatives and Oxygen-deficient
TiO₂ Nanotubes: Identified Charge-transfer Processes and Photo-electric Synergistic Effect**

Honglin Zhang^{a,1}, Meiyong Jia^{b,1}, Jing Tong^{a,1}, Haihao Peng^a, Yiping Xiang^a, Zhaomeng Chen^c,
Zhengyong Xu^d, Zhaohui Yang^a, Weiping Xiong^{a,c,*}

^a College of Environmental Science and Engineering, Hunan University, Changsha 410082, P.R. China;

^b College of Environmental Science and Engineering, Central South University of Forestry and Technology, Changsha 410004, P.R. China;

^c Hunan Boke Environmental Engineering Co. Ltd, Hengyang 421099, PR China;

^d Hunan Modern Environmental Technology Co. Ltd, Changsha 410004, PR China;

* Corresponding author at: College of Environmental Science and Engineering, Hunan University, Changsha, Hunan 410082, China.

Phone & Fax: +86-0731-8882-2829

E-mail address: xiongweiping@hnu.edu.cn (Xiong W.P.)

¹ These authors contributed equally to this article.

Characterization of the electrodes

X-ray diffraction (XRD) experiments were performed on the Bruker AXS D8 diffractometer (Cu K α radiation, wavelength=0.15406 nm) to record the XRD spectrum at a scanning speed of 2°/min in the range of 2 θ from 5 to 90°. Scanning electron microscopy (SEM) and elemental mapping analysis were performed on the ZEISS Sigma 300 instrument, and the internal structure of the photo-electrode was recorded using a transmission electron microscope (FEI Tecnai G2 F20 S-TWIN). X-ray photoelectron spectroscopy (XPS) analysis was performed on the Thermo Scientific K-Alpha instrument with an excitation source of Al K α rays (h ν =1486.6 eV). The Thermo Scientific Nicolet iS20 was used to test wavelengths ranging from 400-4000 cm⁻¹ Fourier transforms infrared spectroscopy (FT-IR) obtained 32 sweeps over the range. The Thermo Scientific Nicolet iS20 was used to test wavelengths ranging from 400-4000 cm⁻¹. Over the range, 32 scans were made to obtain Fourier transform infrared spectroscopy (FT-IR). AFM images were recorded via Czech TESCAN MIRA LMS. Ultraviolet-visible diffuse reflection spectroscopy (DRS) and steady-state/transient fluorescence spectroscopy (PL) were measured by the Varian Cary 300 spectrophotometer and the Edinburgh FLS1000 fluorometer, respectively. Electron paramagnetic resonance (EPR) spectroscopy was obtained on the Bruker EMXPLUS spectrometer.

HPLC analysis operation

The reaction samples were filtered using a 0.22 μ m cellulose acetate injection membrane filter and then TC concentrations were determined employing an Agilent TC-C18 column (4.6 \times 250 mm, 5 μ m) on an HPLC (Agilent 1100 series, USA). The mobile phase was a mixed solution of 20% formic acid solution (volume fraction of 0.1%) and 80% acetonitrile solution.

The mobile phase flow rate and sample injection volumes were $1 \text{ mL}\cdot\text{min}^{-1}$ and $20 \text{ }\mu\text{l}$, respectively. The column temperature was 30°C , and the detector wavelength was set to 357 nm . The sample residence time was 3.7 min .

The liquid chromatography-mass spectrometry analysis operation

The LC-MS system consisting of the 6460 High-Performance Liquid Chromatography (Agilent, USA) and API 3000 mass analyzer was chosen to explore their degradation pathways and intermediates. Mobile phase A (0.1%, formic acid) and mobile phase B (acetonitrile) flowed through a Kromasil C18 column ($4.6 \times 100 \text{ mm}$) from Agilent. The eluate was maintained at a flow rate of $0.3 \text{ mL}\cdot\text{min}^{-1}$ under a positive ion source (ESI), the sample injection volume was $10 \text{ }\mu\text{l}$, and the column temperature was 30°C . The linear gradient elution was as follows: A=95% (1 min), 5% (10 min), 5% (15 min), 95% (20 min), and 95% (25 min), meanwhile, another eluting solvent was acetonitrile, the sum of the two was 100%. The maximum pressure limit of the instrument was 1300 bar.

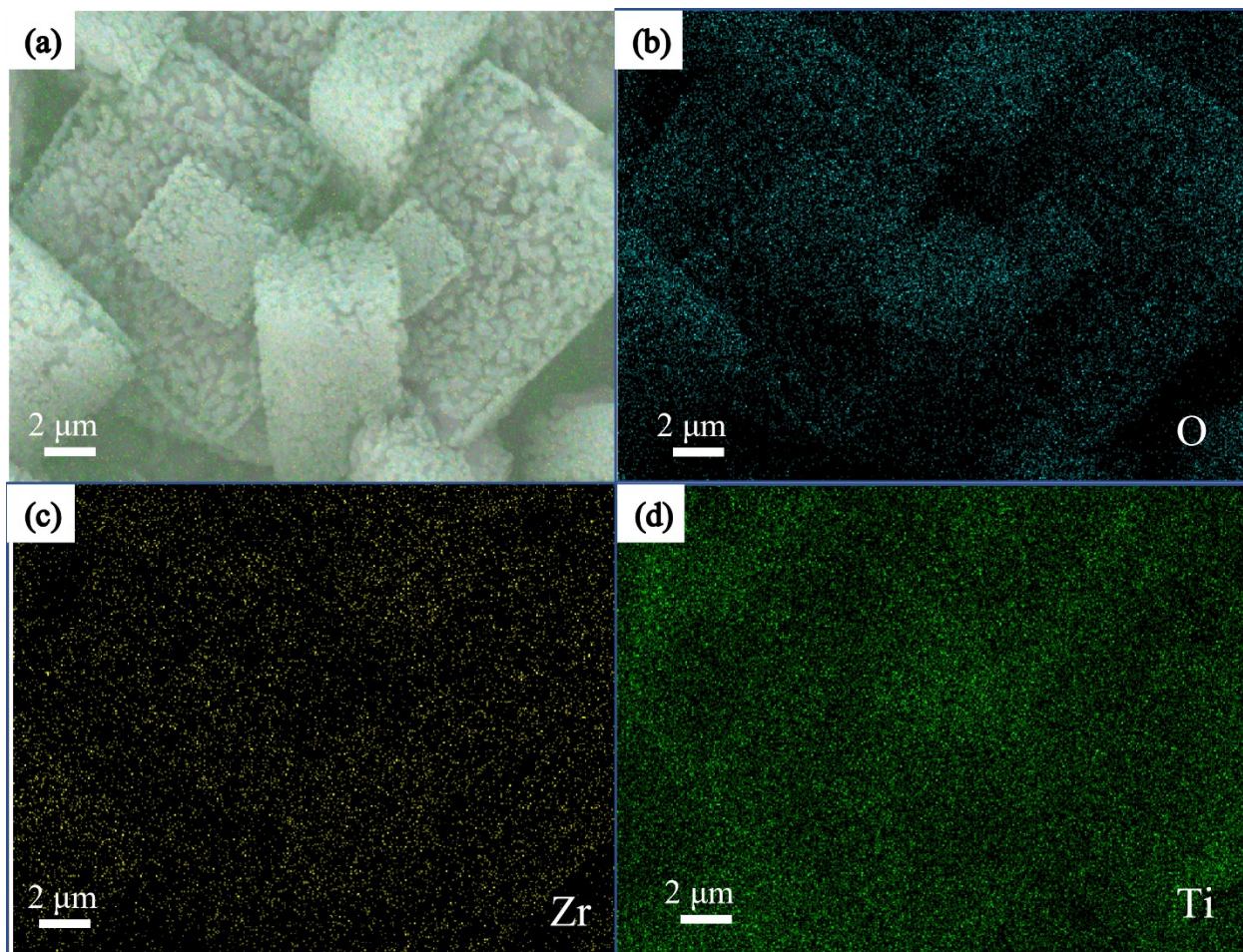


Fig. S1 O, Zr, and Ti mapping of the Ar-ZrO₂/Ti₂O₃-TNTs photo-electrode.

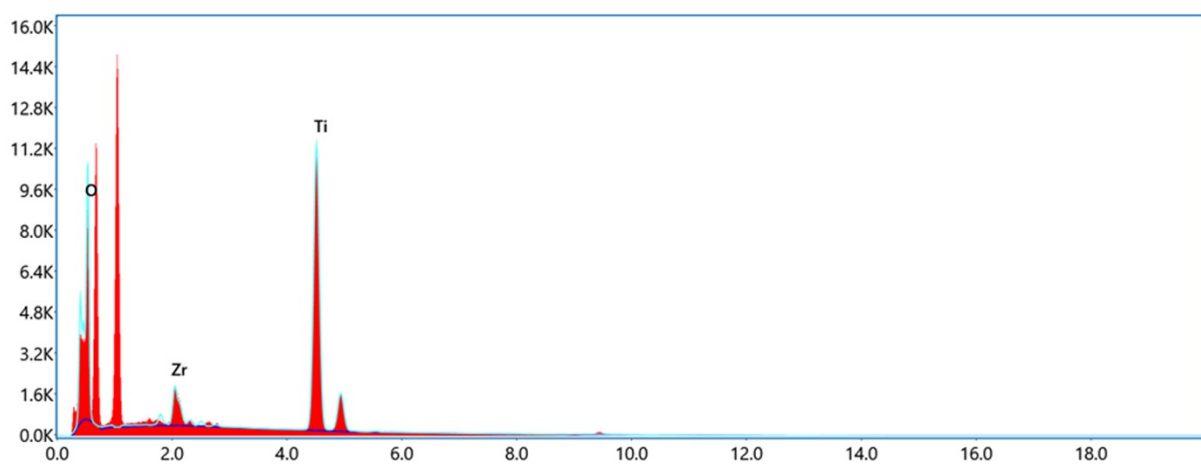


Fig. S2 The load of O, Zr, and Ti elements.

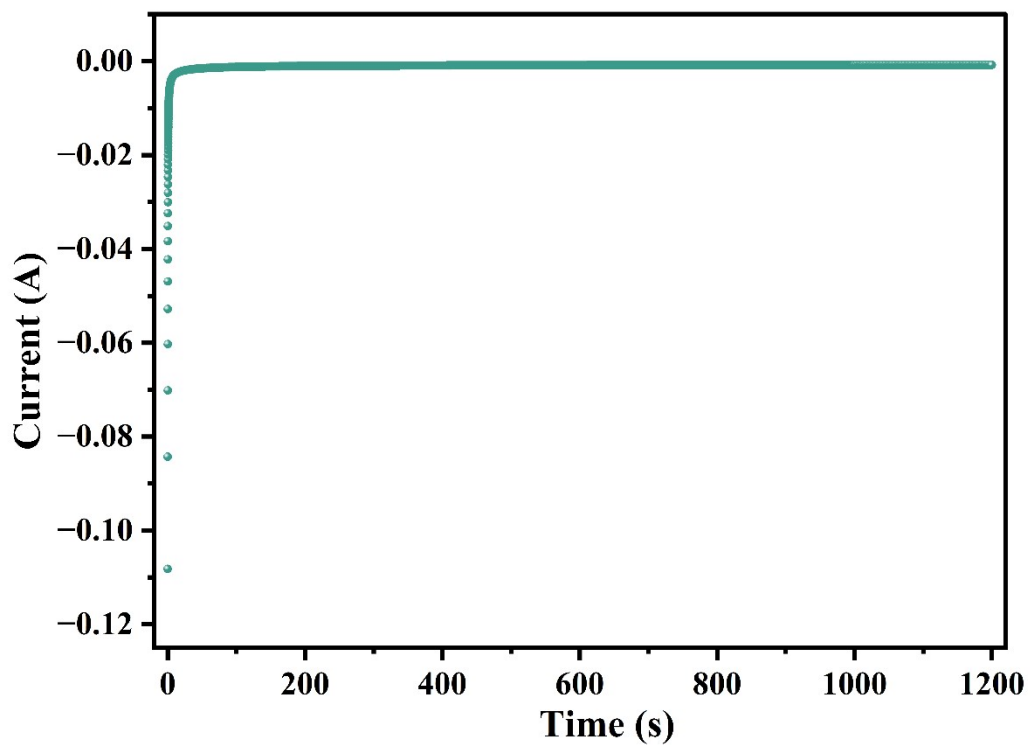


Fig. S3 Electrochemical reduction current-time curve.

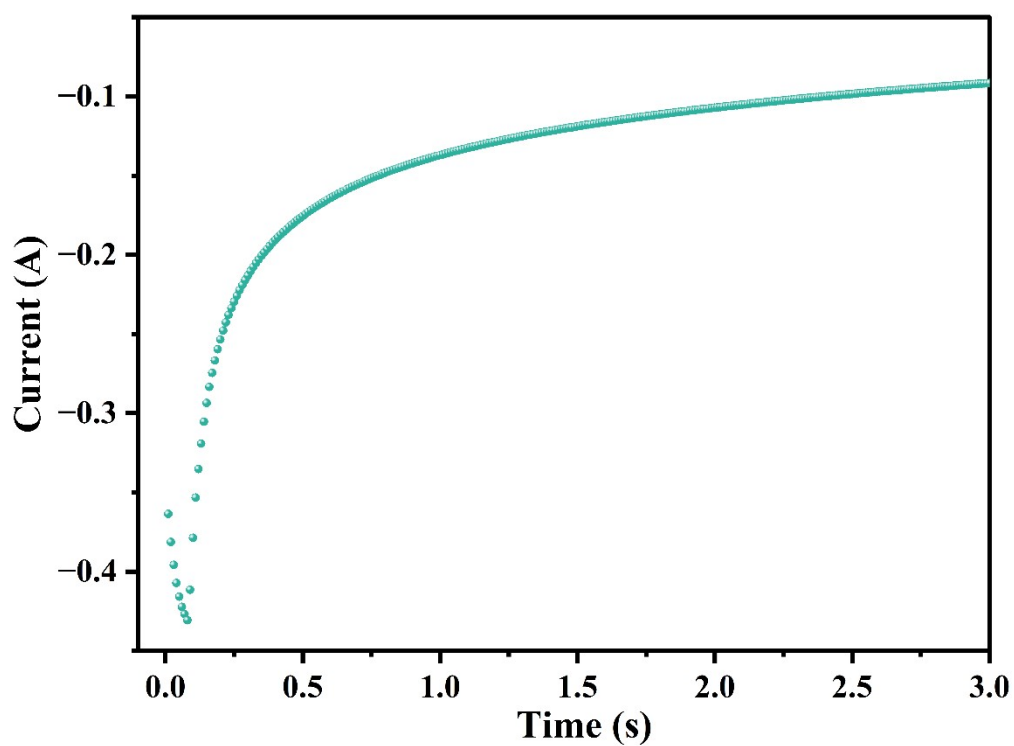


Fig. S4 $(\text{NH}_4)_2\text{SO}_4$ reduction current-time curve.

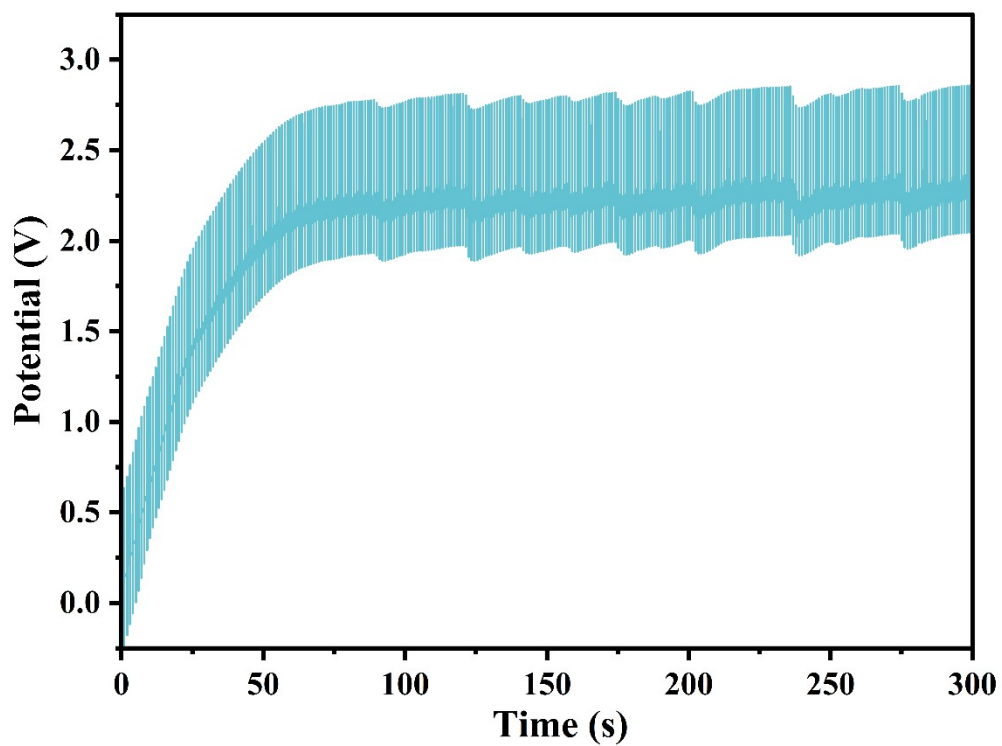


Fig. S5 Pulsed electrodeposition potential-time curve of Zr-Ti₂O₃-TNTs.

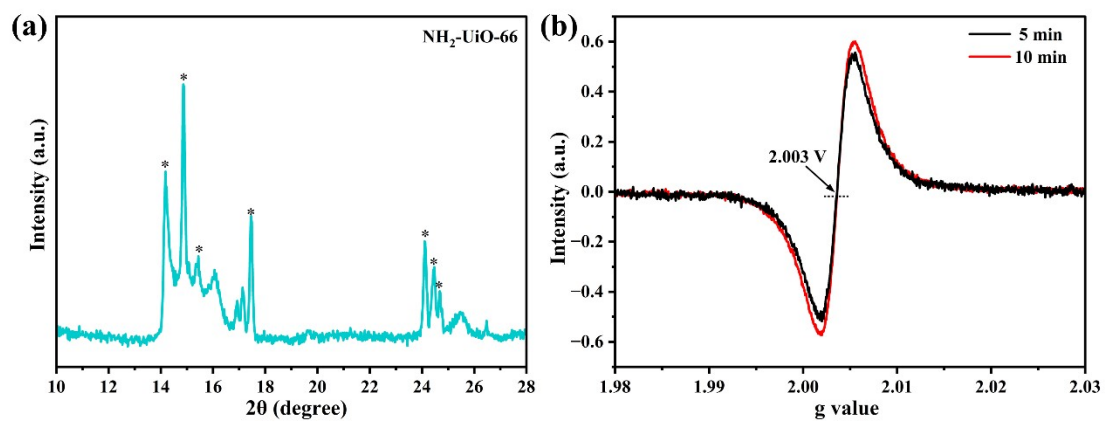


Fig. S6 (a) Characterization of the NH₂-UiO-66 using XRD; (b) The EPR spectra of the Ar-ZrO₂/Ti₂O₃-TNTs photo-electrode.

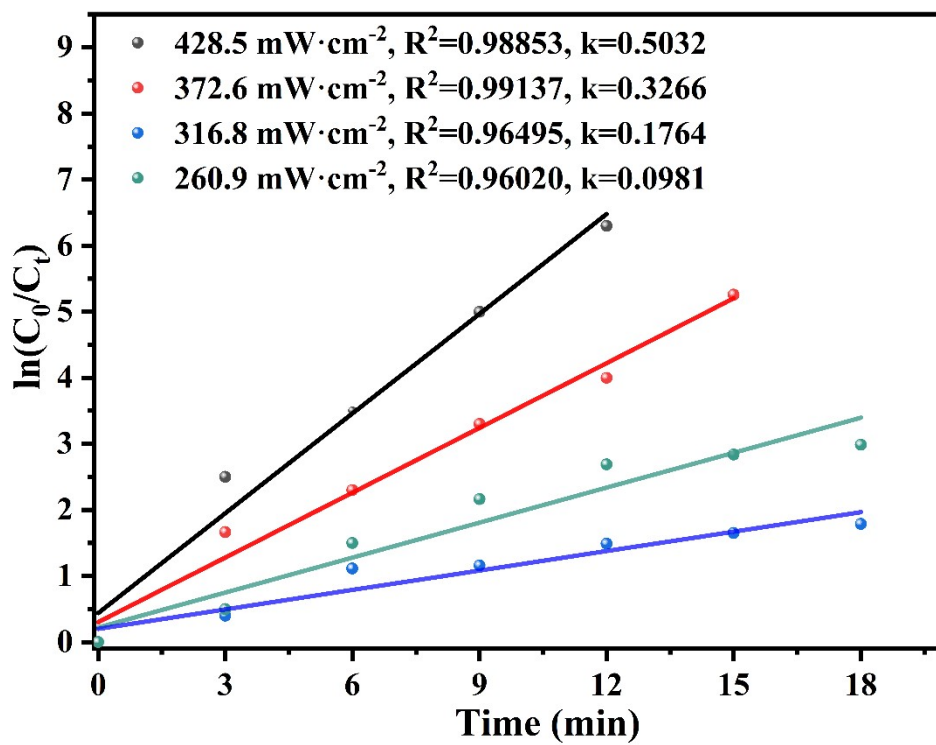


Fig. S7 The first-order reaction kinetic constant of TC degradation at different photon fluxes.

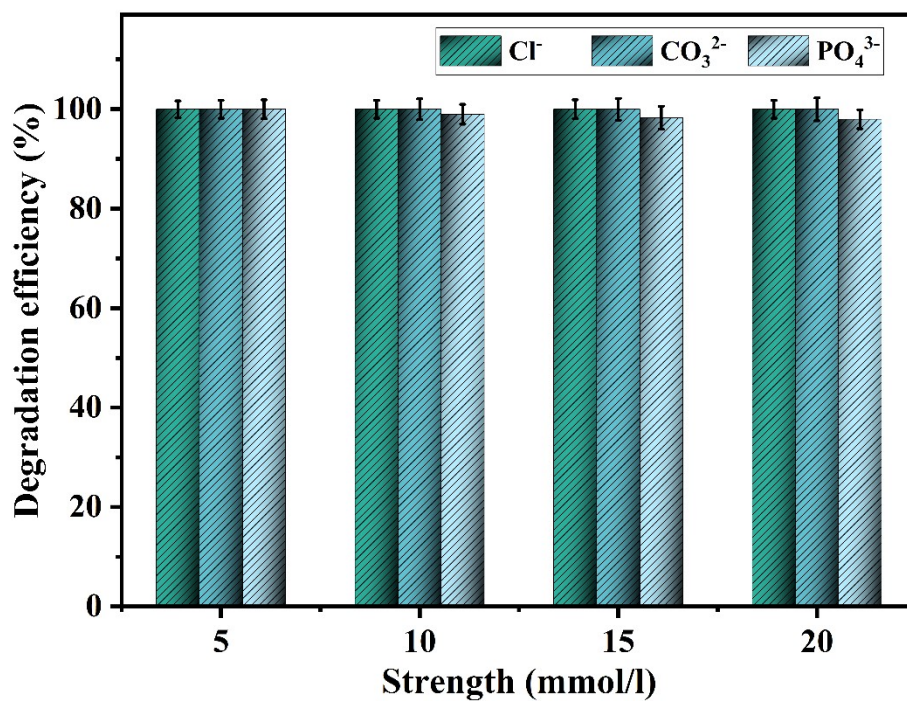


Fig. S8 The effect of ionic strength on TC degradation.

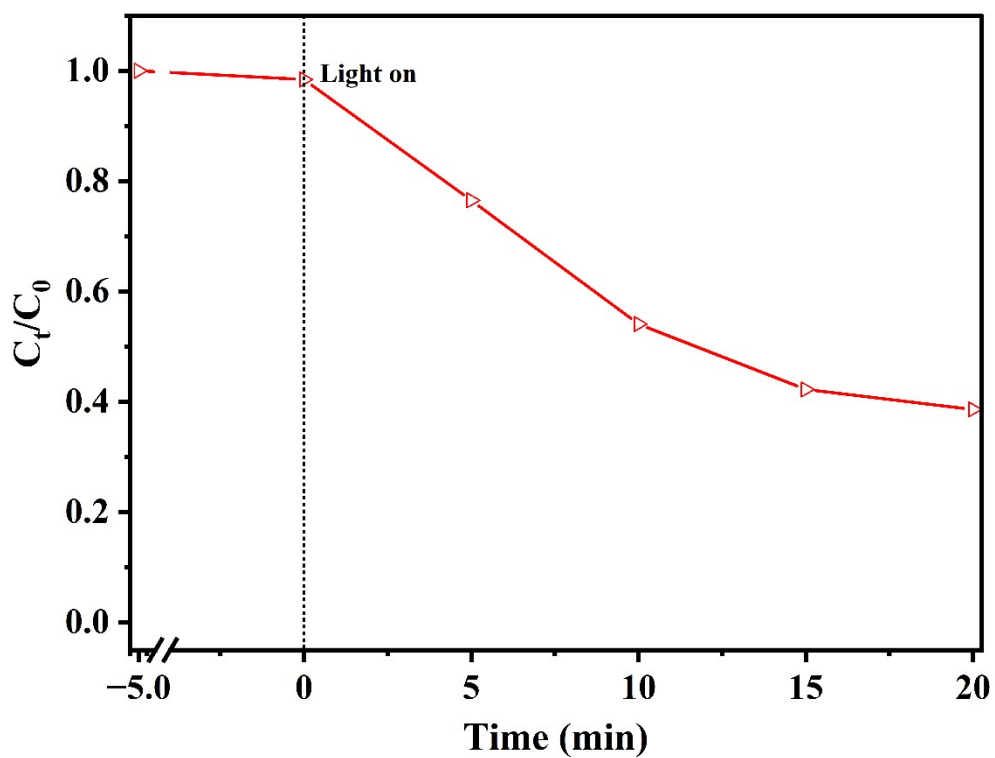


Fig. S9 Mineralization rate of tetracycline degraded by the Ar-ZrO₂/Ti₂O₃-TNTs photo-electrode

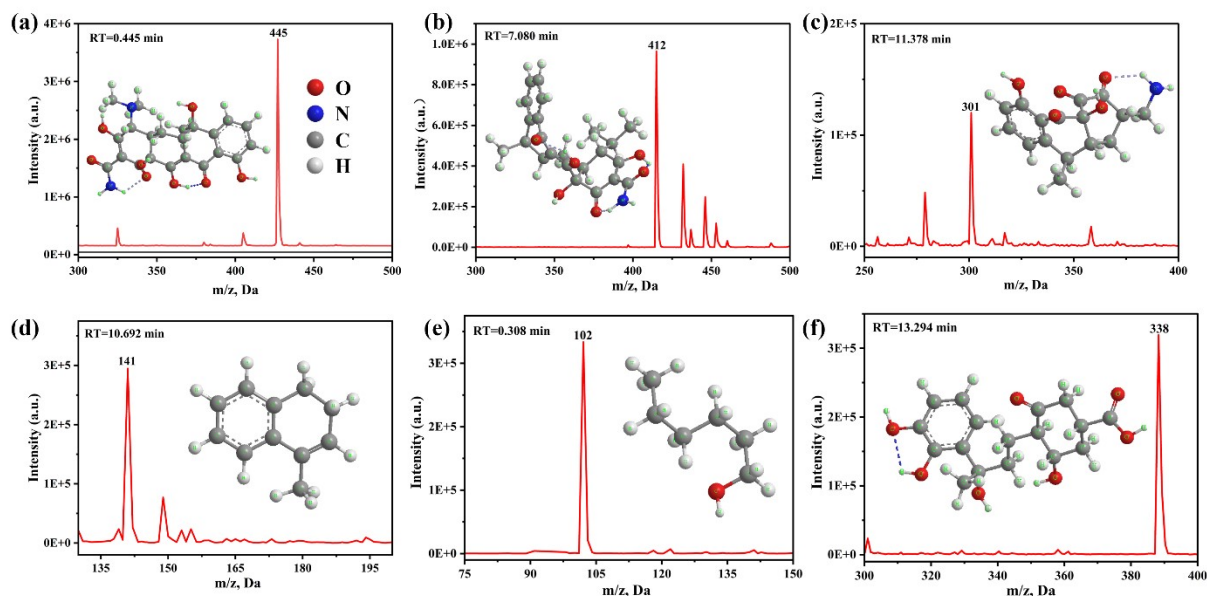


Fig. S10 LC-MS analysis of TC intermediates by the Ar-ZrO₂/Ti₂O₃-TNTs photo-electrode.

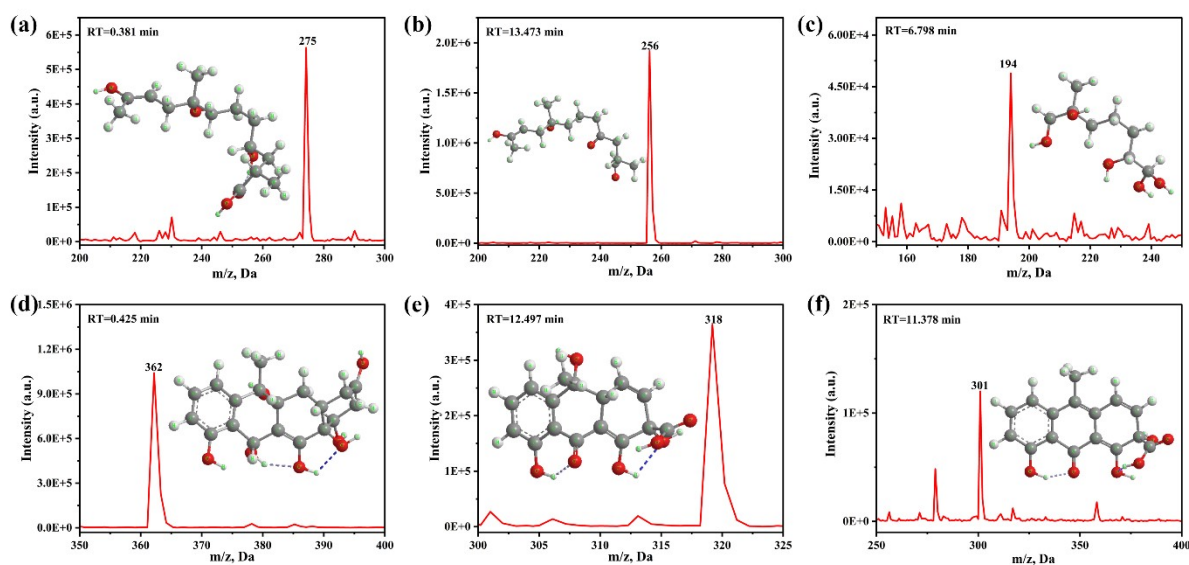


Fig. S11 The intermediates of TC by the Ar-ZrO₂/Ti₂O₃-TNTs photo-electrode.

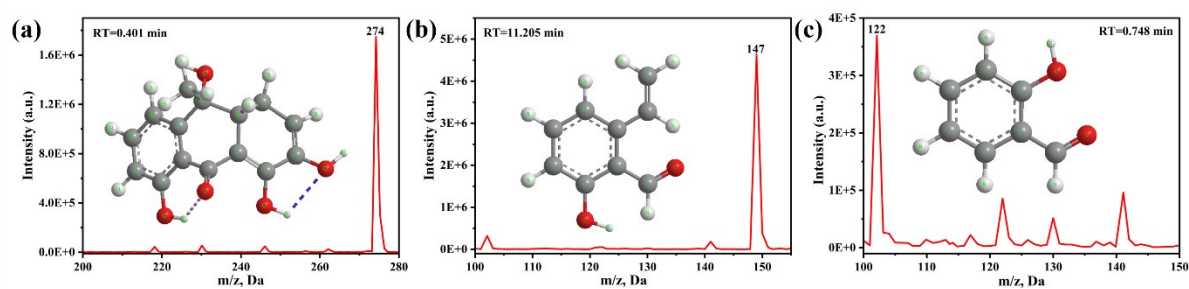
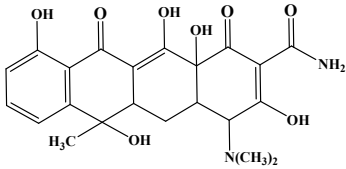
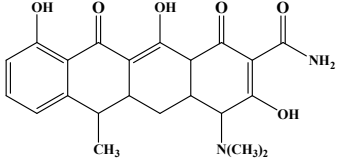
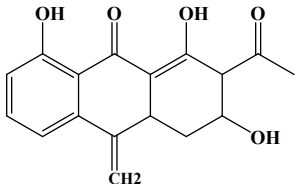
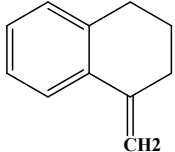
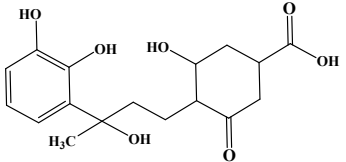
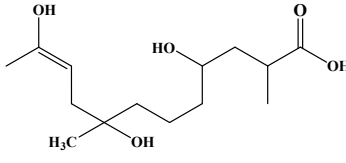
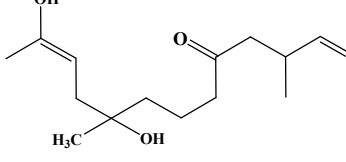
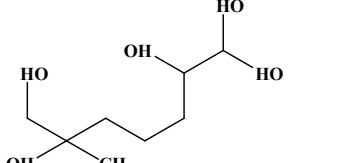
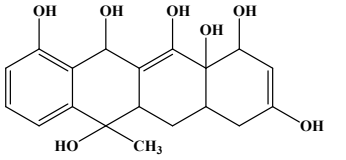


Fig. S12 The intermediates during TC degradation by the Ar-ZrO₂/Ti₂O₃-TNTs photo-electrode.

Table. S1 Information and proposed structure of the degradation intermediates from TC

Products	Molecular Formula	m/z	Proposed Structure
TC	$C_{22}H_{25}N_2O_8$	445	
P1	$C_{23}H_{26}NO_6$	412	
P2	$C_{16}H_{15}NO_5$	301	
P3	$C_{11}H_9$	141	
P4	$C_{16}H_{34}O_7$	338	
P5	$C_{14}H_{27}O_5$	275	
P6	$C_{13}H_{16}O_4$	256	
P7	$C_8H_{18}O_5$	194	
P8	$C_{19}H_{22}O_7$	362	

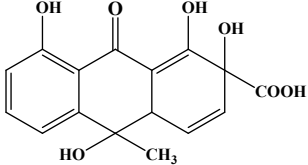
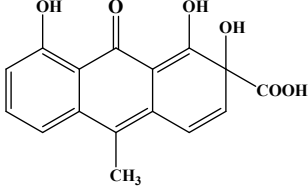
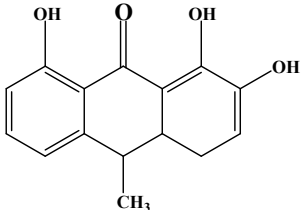
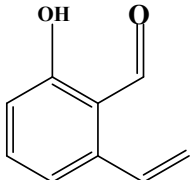
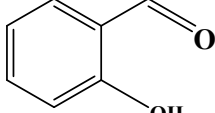
P9	$C_{16}H_{14}O_7$	318	
P10	$C_{16}H_{13}O_6$	301	
P11	$C_{15}H_{14}O_5$	274	
P12	$C_8H_{10}O_2$	147	
P13	$C_7H_6O_2$	122	

Table. S2 The XPS peak data of the NH_2 -UiO-66/ Ti_2O_3 -TNTs photo-electrode

Category	Area	Beginning X	Ending X	FWHM	Center	Height
$Ti^{4+}2p_{1/2}$	151029.30	461.48	467.08	1.98076	464.28	70534.5
$Ti^{4+}2p_{3/2}$	292854.00	456.88	459.98	1.09006	458.48	248405.9
$Ti^{3+}2p_{1/2}$	6783.75	461.48	463.18	0.86835	462.28	7459.0
$Ti^{3+}2p_{3/2}$	11919.38	456.08	458.28	0.80845	457.18	13359.2

Table. S3 The XPS peak data of the Ar-ZrO₂/Ti₂O₃-TNTs photo-electrode

Category	Area	Beginning X	Ending X	FWHM	Center	Height
Ti ⁴⁺ 2p _{1/2}	95593.45	462.48	467.18	1.9808	464.78	44988.0
Ti ⁴⁺ 2p _{3/2}	209903.80	457.28	460.68	1.1736	458.98	165446.0
Ti ³⁺ 2p _{1/2}	30082.96	459.08	462.78	1.9808	460.88	14590.0
Ti ³⁺ 2p _{3/2}	8984.05	456.38	458.48	1.2317	457.38	7162.0

Table. S4 Full-hole parameters of various electrodes.

Sample	S _{BET} (m ² /g) ^a	S _{micro} (m ² /g) ^b	S _{meso} (m ² /g) ^c	V _{total} (m ³ /g) ^d	V _{micro} (m ³ /g) ^e	D(nm) ^f
TNTs ¹	1.0043	0.0957	0.9086	0.0015	0.0003	4.3260
Ti ₂ O ₃ -TNTs ¹	1.2634	0.0546	1.2088	0.0016	0.0002	4.3008
Zr-Ti ₂ O ₃ -TNTs ¹	1.6320	0	1.6320	0.0013	0	3.8706
NH ₂ -UiO-66/Ti ₂ O ₃ - TNTs	0.38310	0.3538	0.0293	0.00167	0.000128	23.1811
Ar-ZrO ₂ /Ti ₂ O ₃ -TNTs	1.26290	0.2227	1.0402	0.00624	0.000076	18.9114

^a BET-specific surface.

^b Micropore BET calculated using the t-plot method.

^c Mesopore BET calculated using the t-plot method.

^d Total pore volume measured at P/P₀= 0.995.

^e Micropore volume calculated using the t-plot method.

^f The pore diameter calculated from the desorption branch of the isotherm using.

- Related references

1. M.Y Jia, Q. Liu, W.P. Xiong, Z.H. Yang, C. Zhang, D.B. Wang, Y.P. Xiang, H.H Peng, J. Tong, J. Cao, H.Y. Xu, Ti^{3+} self-doped TiO_2 nanotubes photoelectrode decorated with Ar- Fe_2O_3 derived from MIL-100(Fe): Enhanced photo-electrocatalytic performance for antibiotic degradation, *Applied Catalysis B: Environmental*, 2022, DOI: 10.1016/j.apcatb.2022.121344.